Specifics of Thermophysical Properties and Heat Transfer at Supercritical Pressures in Power-Engineering Applications: A Review

Igor L. Pioro
Faculty of Energy Systems and Nuclear Science
University of Ontario Institute of Technology
2000 Simcoe Str. North, Ontario, L1H 7K4, Canada
Tel.: 1-905-721-8668 ext. 5528, Fax: 1-905-721-3046
*Igor.Pioro@uoit.ca

ABSTRACT
Currently, SuperCritical Fluids (SFCs) are used in various industries worldwide. The largest application of SCFs by scale is the use of SuperCritical Water (SCW) in a power cycle of coal-fired power plants. Using SuperCritical Pressure (SCP) Rankine "steam" cycle allows to reach gross thermal efficiencies of a plant up to 55%, which is the second highest value achieved in power industry. On contrary, current subcritical-pressure water-cooled Nuclear Power Plants (NPPs) of Generations-II and III have significantly lower gross thermal efficiencies within the range of 30–36% (up to 37–38% for Generation-III$^+$ NPPs). To increase efficiency of next generation – Generation-IV NPPs higher parameters (mainly temperature, but in some cases also pressure) should be reached for reactors' coolants and corresponding to that power cycles.

Analysis of Generation IV nuclear-reactor concepts shows that three concepts will be cooled with SCFs such as helium and water, and there is a possibility that other concepts will be linked to a SCP Rankine cycle or to a SCP Brayton cycle with helium, helium-nitrogen-mixture, or carbon-dioxide working fluids. Therefore, specifics of thermophysical properties and heat transfer / hydraulic resistance of SCFs are very important for reliability and safety of new thermal and nuclear power plants. Also, for SCW nuclear reactors heat transfer to SCW flowing inside bundle geometries has to be estimated.

1. INTRODUCTION

It is well known that electrical-power generation is the key factor for advances in industry, agriculture, technology, and the standard of living (see Table 1 and Fig. 1) [1]. Also, strong power industry with diverse energy sources is very important for a country's independence. In general, electrical energy can be generated from: 1) non-renewable energy sources such as coal, natural gas, oil, and nuclear; and 2) renewable energy sources such as hydro, biomass, wind, geothermal, solar, and marine power. Today, the main sources for electrical-energy generation (see Fig. 2) are: 1) thermal power – primarily using coal and secondary using natural gas; 2) "large" hydro-electric power plants; and 3) nuclear power. The balance of the energy sources is from using oil, biomass, wind, geothermal and solar, and have visible impact just in selected countries.

Gross thermal efficiencies of modern thermal and Nuclear Power Plants (NPPs) are listed in Table 2. Figures 3–6 show simplified Temperature-Specific Entropy diagrams for: 1) Pressurized-Water-Reactor (PWR) NPP (PWRs are the largest group of nuclear-power reactors

in the world – 65% or 292 units from 450 nuclear-power reactors [1]) (Fig. 3); 2) Sodium-cooled-Fast-Reactor (SFR) NPP (currently, only two reactors operate in the world) (Fig. 4); 3) Advanced Gas-cooled Reactor (AGR) NPP (Fig. 5); and 4) SuperCritical Pressure (SCP) coal-fired thermal power plant (Fig. 6).

Table 1. Population, Electrical Energy Consumption (EEC) and Human Development Index (HDI) in selected countries [1]. Data for all countries in the world are listed in [1].

No	Country	Population in millions (Jan. 2018)	Electrical Energy Consumption (EEC)		Rank (2015)	HDI (2015)
			TW h (2016)	Watts per Capita		
1	Norway	5.35	149.5	3190	1	0.949
2	Australia	24.77	256.9	1184	2	0.939
3	Germany	82.29	648.4	899	4	0.926
4	USA	326.77	4350.8	1520	10	0.920
5	Canada	36.95	663.0	2048	10	0.920
6	UK	66.57	338.6	581	16	0.909
7	Japan	127.19	999.6	897	17	0.903
8	France	65.23	553.4	968	21	0.897
9	Russia	143.96	1087.1	862	49	0.804
10	Brazil	210.87	581.7	315	79	0.754
11	China	1415.05	6142.5	496	90	0.738
12	World (see Fig. 1)	7606.68	24 816.4	372	102	0.717
13	India	1400.05	1400.8	114	131	0.624
14	Niger	22.31	0.2 (2005)	1.0	187	0.353
15	Central African Republic	4.74	0.1 (2005)	2.4	188	0.352

* $\text{EEC}/\ \frac{\text{W}}{\text{Capita}} = \frac{\left(EEC,\ \frac{TW\,h}{year}\right) \times \frac{10^{12}}{365\ \text{days} \times 24\ \text{h}}}{(\text{Population},\ \ \text{Millions}) \times 10^{6}}$.

** HDI – Human Development Index by United Nations (UN); HDI is a comparative measure of life expectancy, literacy, education and standards of living for countries worldwide. HDI is calculated by the following formula: $\text{HDI}= \sqrt[3]{\text{LEI}\times\text{EI}\times\text{II}}$, where LEI – Life Expectancy Index, EI - Education Index, and II – Income Index. It is used to distinguish whether the country is a developed, a developing, or an under-developed country, and also to measure the impact of economic policies on quality of life.

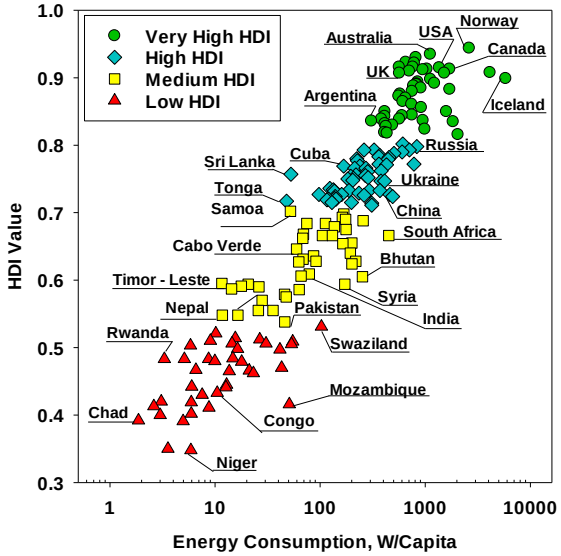

Fig. 1. Impact of EEC on HDI for all countries of the world [1].

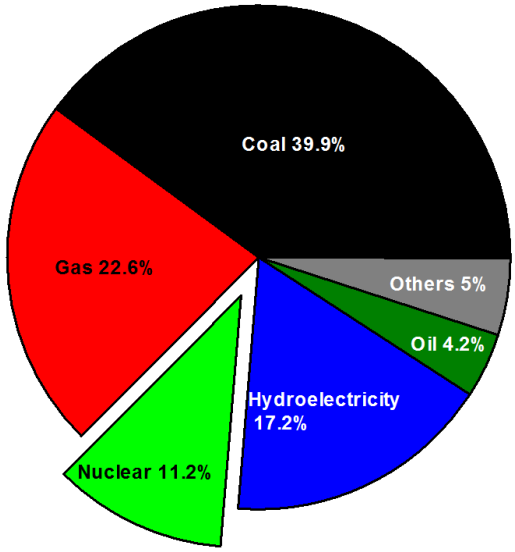

Fig. 2. World electricity generation by source [1].

Table 2. Typical ranges of thermal efficiencies (gross[1]) of modern thermal and NPPs [1].

No	Power Plant	Gross Eff. %
1	Combined-cycle power plant (combination of Brayton gas-turbine cycle (fuel - natural gas; combustion-products parameters at gas-turbine inlet: $T_{in} \approx 1650$°C) and Rankine steam-turbine cycle (steam parameters at the turbine inlet: $T_{in} \approx 620$°C (T_{cr} = 374°C)).	Up to 62
2	**Supercritical-pressure** coal-fired thermal power plant (new plants) (Rankine-cycle steam inlet turbine parameters (for *T-s* diagram – see Fig. 6 and for plant layout – Fig. 7): $P_{in} \approx 23.5 – 38$ MPa (P_{cr} = 22.064 MPa), $T_{in} \approx 540$ - 625°C (T_{cr} = 374°C) and $T_{reheat} \approx 540$ - 625°C).	Up to 55
3	Subcritical-pressure coal-fired power plant (older plants) (Rankine-cycle steam (*T-s* diagram is similar to that shown in Fig. 5): $P_{in} \approx 17$ MPa, $T_{in} \approx$ 540°C (T_{cr} = 374°C) and $T_{reheat} \approx 540$°C).	Up to 43
4	Advanced Gas-cooled Reactor (AGR) (carbon-dioxide-cooled) NPP (Generation-III) (reactor coolant: P=4 MPa & T=290-650°C; steam (for *T-s* diagram – see Fig. 5): P=17 MPa (T_{sat}=352°C) & T_{in}=560°C)	Up to 42
5	Sodium-cooled Fast Reactor (SFR) (BN-600 / BN-800) NPP (steam (for *T-s* diagram – see Fig. 4): P=14 MPa (T_{sat}=337°C) & T_{in}=505°C)	Up to 40
6	Pressurized Water Reactor (PWR) NPP (Generation-III and III$^+$) (reactor coolant: P=15.5 MPa & T_{out}=327°C; steam (for *T-s* diagram – see Fig. 3): P=7.8 MPa & T_{in}=293°C)	Up to 38
7	Boiling Water Reactor (BWR) NPP (Generation-III, current fleet) (P_{in}=7.2 MPa & T_{in}=288°C); steam has approximately same parameters at turbine inlet	Up to 34

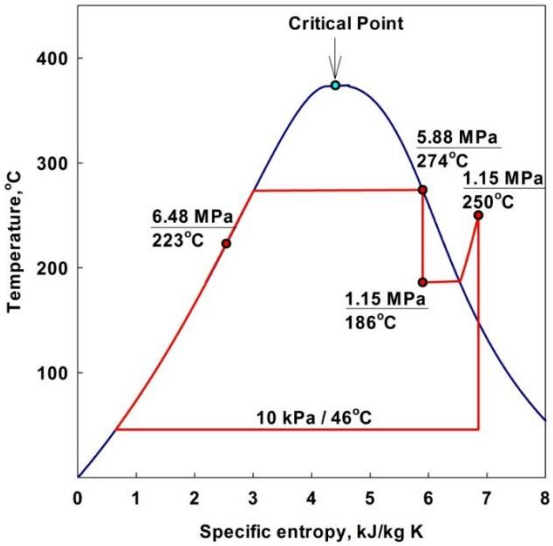

Fig. 3. Simplified *T-s* diagram of generic PWR NPP [1].

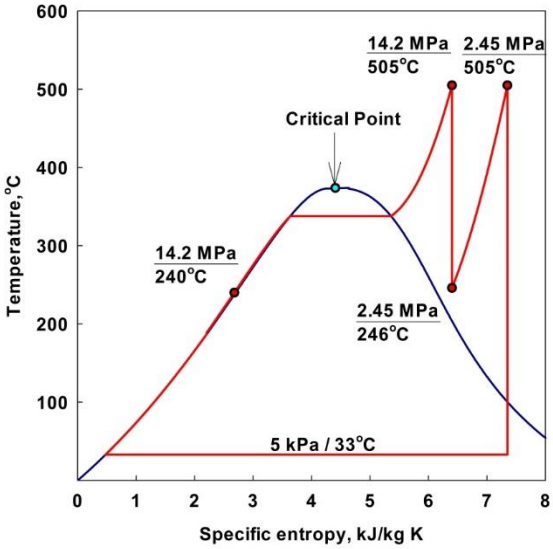

Fig. 4. Simplified *T-s* diagram for the 600-MW$_{el}$ BN-600 SFR NPP [1].

[1] Gross thermal efficiency of a unit during a given period of time is the ratio of the gross electrical energy generated by a unit to the thermal energy of a fuel consumed during the same period by the same unit. The difference between gross and net thermal efficiencies includes internal needs for electrical energy of a power plant, which might be not so small (5% or even more).

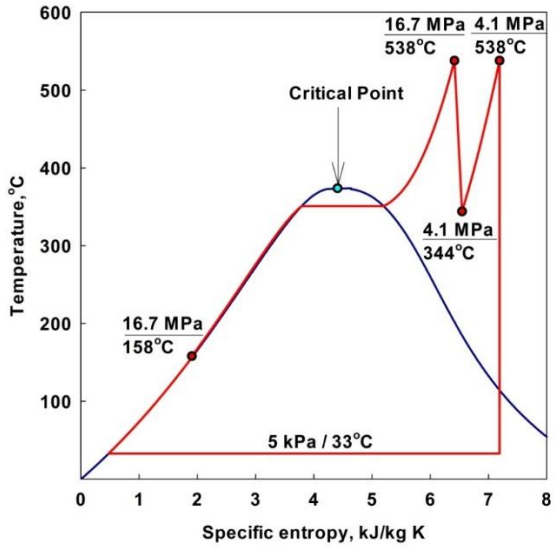

Fig. 5. Simplified *T-s* diagram of generic AGR NPP [1].

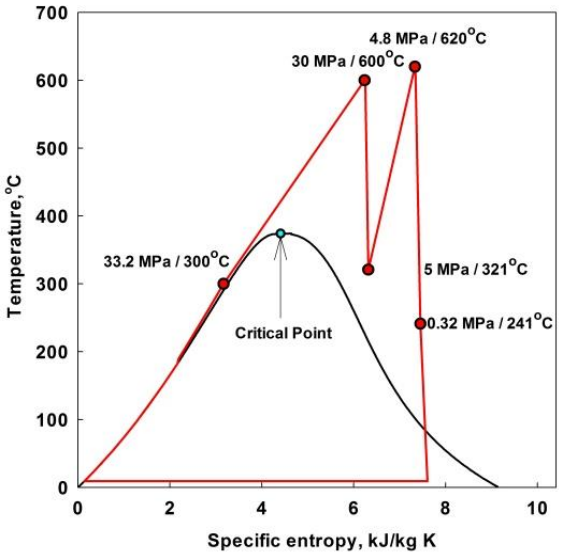

Fig. 6. Simplified *T–s* diagram of generic SCP coal-fired power plant [1]. For plant layout – see Fig. 7.

2. SUPERCRITICAL-PRESSURE THERMAL POWER PLANTS

For more than 100 years, coal was and still is used for generating electrical energy at thermal-power plants worldwide (see Fig. 2). All coal-fired power plants operate based on, the so-called, steam Rankine cycle, which can be setup at two different levels of pressures: 1) older or smaller capacity power plants operate at subcritical steam pressures no higher than 16-18 MPa (*T-s* diagram is similar to that shown in Fig. 5); and 2) modern large capacity power plants operate at SCPs within the range of 23.5–38 MPa (see Figs. 6 and 7) [1, 2]. Supercritical pressures refer to pressures above the critical pressure of water, which is 22.064 MPa (see Table 3).

Table 3. Basic properties of helium, carbon dioxide, and water.

No	Properties	Fluids		
		Helium	**Carbon Dioxide**	**Water**
1	Chemical formula	He	CO_2	H_2O
2	Molar mass, kg/kmol	4.0026	44.01	18.015
3	Triple point, °C	–270.97	–56.558	0.01
4	Normal boiling-point temperature, °C	–268.93	–78.464	99.974
5	Critical point temperature, °C	–267.95	30.978	373.95
6	Critical point pressure, MPa	0.2276	7.3773	22.064
7	Critical point density, kg/m^3	72.567	467.6	322.0

It is well-known that the driving force in thermal-power industry for long time, and, nowadays, in nuclear-power industry, is thermal efficiency. In general, theoretical thermal efficiency, i.e., of a Carnot ideal engine, depends solely on the difference between the hot and cold temperature reservoirs. Therefore, mainly higher temperatures (and pressures) at a gas or steam turbine inlet lead to higher thermal efficiencies of a power cycle. Due to this, about 60 years ago, thermal power industry has moved from subcritical-pressure-steam Rankine cycle to SCP one (see Table 2). Nowadays, all large capacity modern coal-fired power plants are SCP ones (here we are talking about hundreds of units worldwide). And, currently, this is the largest by scale application of SuperCritical Fluids (SCFs), in particular, SuperCritical Water (SCW), in industry.

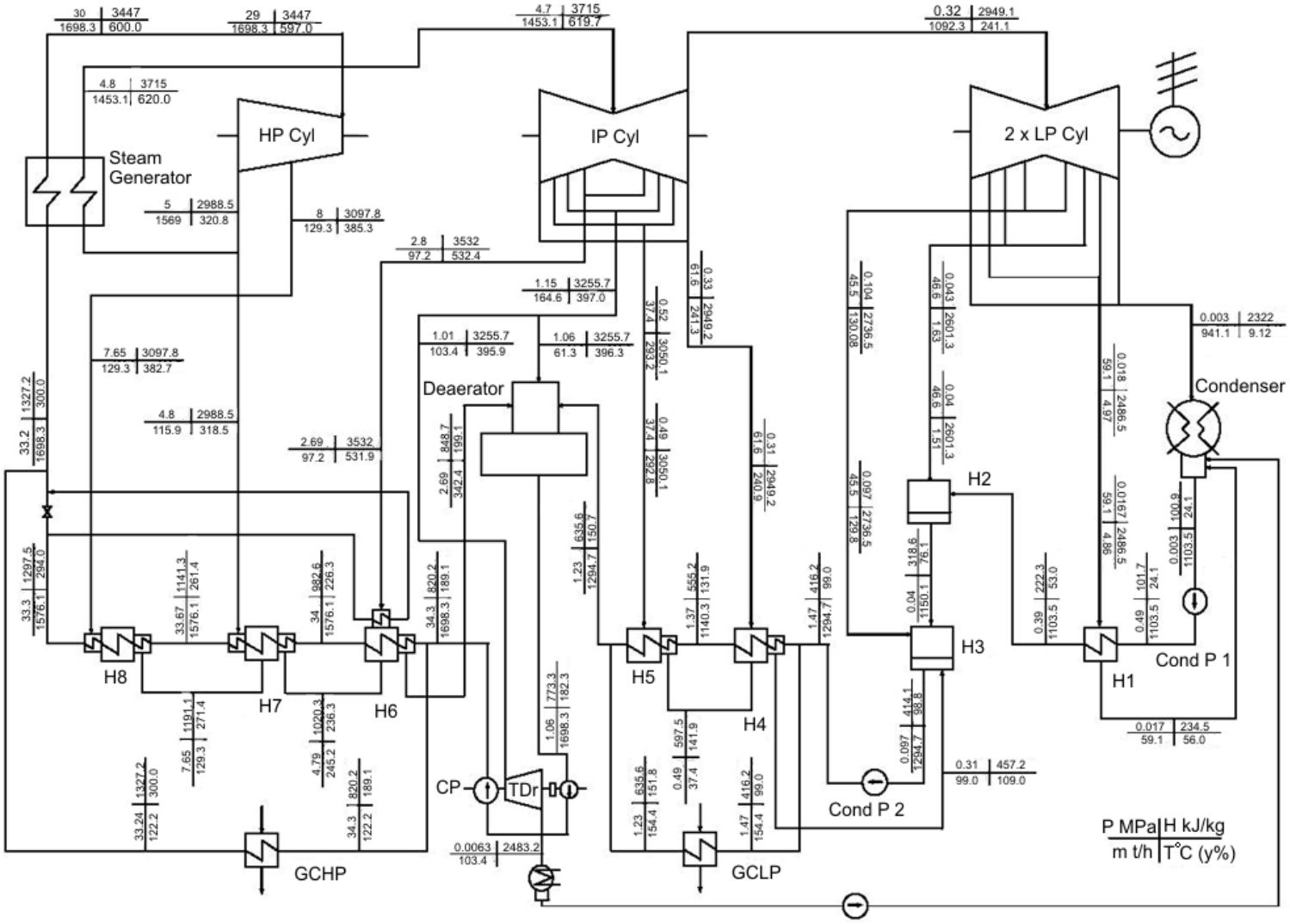

Fig. 7. Supercritical-pressure single-reheat regenerative cycle 600-MW_{el} Tom'-Usinsk thermal power plant (Russia) layout [1]: Cond P – Condensate Pump; CP – Circulation Pump; Cyl – Cylinder; GCHP – Gas Cooler of High Pressure; GCLP – Gas Cooler of Low Pressure; H – Heat exchanger (feedwater heater); HP – High Pressure; IP – Intermediate Pressure; LP – Low Pressure; and TDr – Turbine Drive.

However, despite all advances in coal-fired power-plants design and operation worldwide, they are still considered as not of minimum environmental impact due to significant carbon-dioxide emissions[2] and air pollution as a result of the combustion process. In addition, coal-fired power-plants produce also virtual mountains of slag and ash, and other gas emissions may contribute to acid rains. Therefore, eventually, they should be replaced with more "environmentally-friendly" power plants, e.g., NPPs, which don't emit carbon dioxide into atmosphere.

3. NUCLEAR POWER PLANTS

Although nuclear power is often considered to be a non-renewable-energy source as the fossil fuels, like coal and gas, nuclear resources can be used for significantly longer or even indefinite time than some fossil fuels, especially, if recycling of unused or spent uranium fuel, thoria-fuel resources, and fast reactors are used. Major advantages of nuclear power [1] are as the following: 1) Concentrated and reliable source of almost infinite energy independent of Mother Nature; 2) High capacity factors[3] are achievable, often in excess of 90% with long operating cycles, making units suitable for continuous base-load operation; 3) Essentially negligible operating emissions of carbon dioxide into atmosphere compared to alternate fossil-fuel thermal power plants; and 4) Relatively small amount of fuel required compared to that of fossil-fuel thermal power plants. Therefore, this source of energy is considered as the most viable one for electrical generation within next 50 – 100 years.

The vast majority of NPPs are equipped with water- or heavy-water-cooled reactors (96% of all nuclear-power reactors in the world or 434 units from 450 nuclear-power reactors), which linked to subcritical-pressure saturated-steam Rankine cycle (see Table 2 and Fig. 3). In general, as of today, no SCPs are used in nuclear-power industry.

In spite of all current advances in nuclear power, NPPs have the following deficiencies: 1) Generate radioactive wastes; 2) Have relatively low thermal efficiencies, especially, NPPs equipped with water-cooled reactors (up to 1.6 times lower than that for modern advanced thermal power plants (see Table 2); 3) Risk of radiation release during severe accidents; and 4) Production of nuclear fuel is not an environment-friendly process. Therefore, all these deficiencies should be addressed in next generation – Generation-IV reactors and NPPs (see Figs. 8 and 9, and Table 4).

In general, there are six concepts of Generation IV nuclear-power reactors and, corresponding to that, NPPs (see Table 4 and Figs. 8 and 9) [1]. All these reactors are high temperature reactors. Moreover, three concepts: 1) VHTR; 2) GFR; and 3) SCWR will use reactor coolants (helium and water) at SCPs (see Tables 3 and 4, and Figs. 8 and 9). On the top of that all six concepts or, at least, a number of them will be linked to SCP power cycles such as Brayton gas-turbine cycle with helium, nitrogen-helium-mixture, or carbon-dioxide working fluids (see Table 4 and Fig. 8) or Rankine "steam"-turbine power cycle (see Table 4 and Figs. 6 and 9). Due to this all these Generation-IV NPPs (see Table 4) will have significantly higher thermal efficiencies comparable with those of combined-cycle and SCP-Rankine-cycle thermal power plants (see Table 2).

---

[2] For example, the largest in the world 5,780-MW_{el} Taichung coal-fired power plant (Taiwan) is the world's largest emitter of carbon dioxide with over 40 million tons per year [1].

[3] The net capacity factor of a power plant is the ratio of the actual output of a power plant over a period of time (usually during a year) and its potential output if it had operated at full nameplate capacity the entire time. To calculate the capacity factor, the total amount of energy a plant produced during a period of time should be divided by the amount of energy the plant would have produced at full capacity. Capacity factors vary significantly depending on the type of a plant.

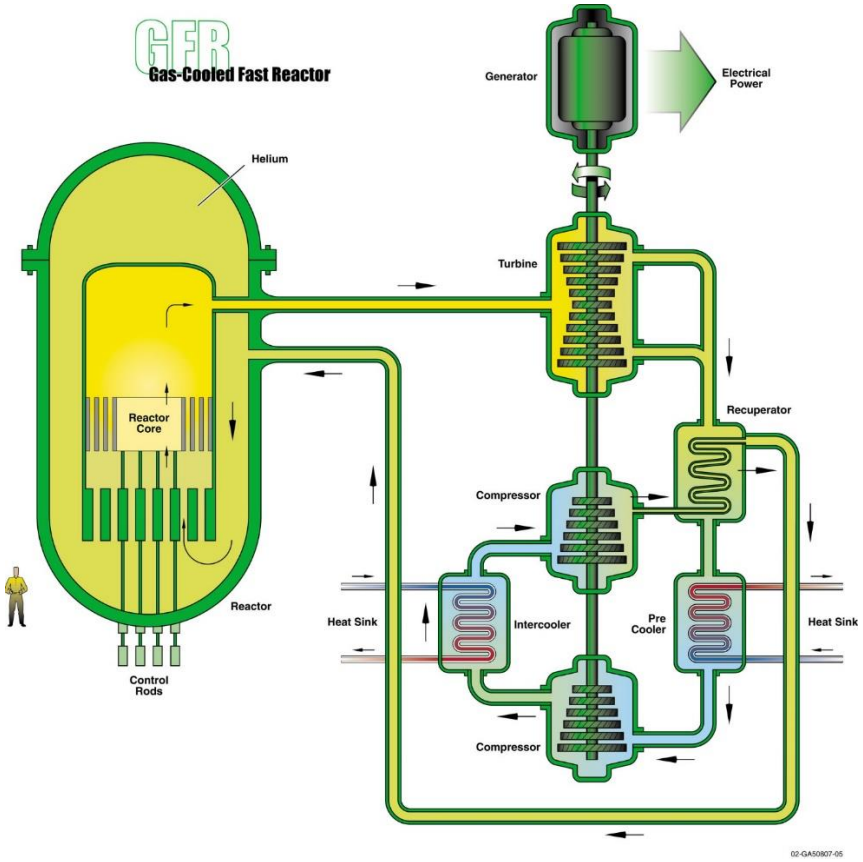

Fig. 8. Gas-cooled Fast Reactor (GFR): Helium-gas-cooled, fast-neutron-spectrum reactor with closed fuel cycle and outlet temperature about 850°C (shown with direct gas-turbine Brayton power cycle) (courtesy of GIF) [1].

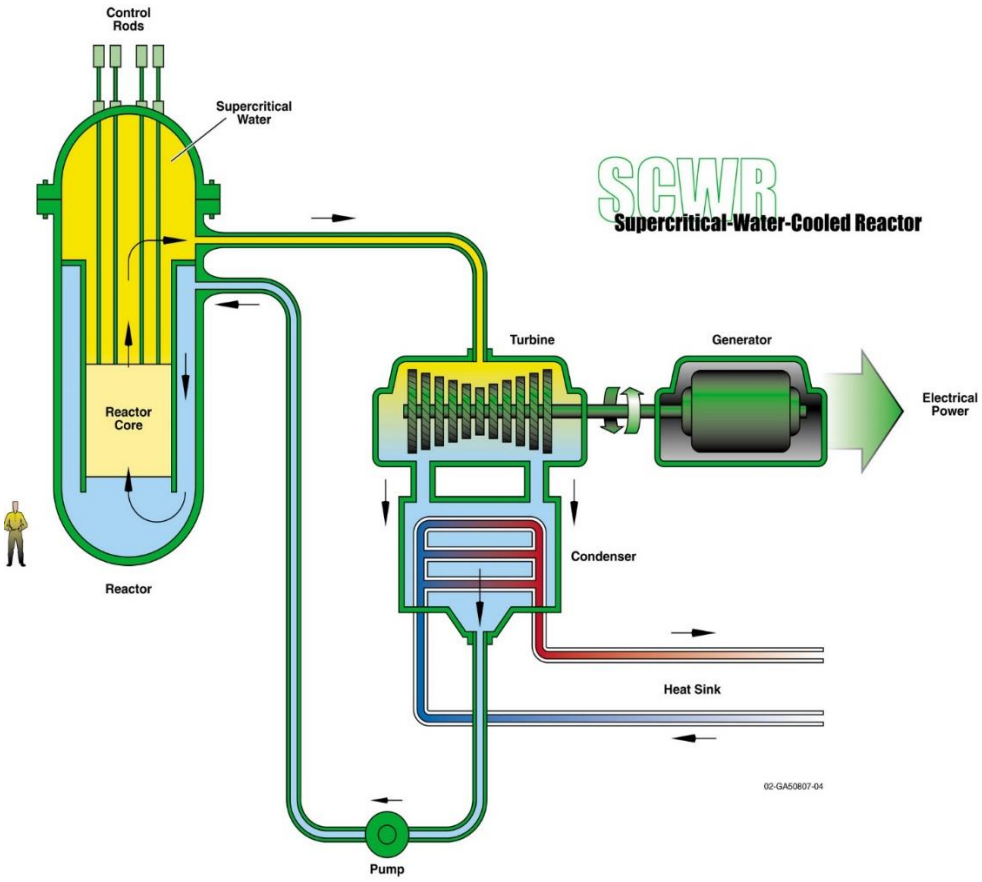

Fig. 9. SuperCritical Water-cooled Reactor (SCWR): Supercritical water-cooled, thermal-neutron-spectrum reactor with outlet temperatures within 510 – 625°C (shown with direct SCP "steam"-turbine Rankine power cycle similar to that of SCP coal-fired power plant (see Figs. 6 and 7)) (courtesy of GIF) [1].

Table 4. Estimated ranges of thermal efficiencies (gross) of Generation-IV NPP concepts (Generation-IV concepts are listed according to thermal-efficiency decrease) [1, 5].

No	Nuclear Power Plant	Gross Eff., %
1	Very High Temperature Reactor (VHTR) NPP (reactor coolant – **SCP helium**: P=7 MPa and T_{in}/T_{out}=640/1000°C; primary power cycle – direct **SCP Brayton gas-turbine cycle**; possible back-up – indirect **SCP Brayton or combined cycles**).	≥55
2	Gas-cooled Fast Reactor (GFR) (Fig. 8) or High Temperature Reactor (HTR) NPP (reactor coolant – **SCP helium**: P=9 MPa and T_{in}/T_{out}=490/850°C; primary power cycle – direct **SCP Brayton gas-turbine cycle**; possible back-up – indirect Brayton or combined cycles).	≥50
3	**SuperCritical Water-cooled** Reactor (SCWR) NPP (Fig. 9) (one of Canadian concepts; reactor coolant – light water: P=25 MPa and T_{in}/T_{out}=350/625°C (T_{cr}=374°C); direct **SCP Rankine "steam" cycle** with high-temperature steam superheat (similar to that of SCP coal-fired power plant (see Figs. 6 and 7)); high-temperature steam superheat: T_{out}=625°C; possible back-up – indirect SCP Rankine "steam" cycle.	45–50
4	Molten Salt Reactor (MSR) NPP (reactor coolant – sodium-fluoride salt with dissolved uranium fuel: T_{in}/T_{out}=700/800°C; primary power cycle – indirect **SCP carbon-dioxide Brayton gas-turbine cycle**; possible back-up – indirect Rankine steam cycle).	~50
5	Lead-cooled Fast Reactor (LFR) NPP (Russian design BREST-OD-300: reactor coolant – liquid lead: P≈0.1 MPa and T_{in}/T_{out}=420/540°C; primary power cycle – indirect subcritical-pressure Rankine steam cycle: P_{in}≈17 MPa (P_{cr}=22.064 MPa) and T_{in}/T_{out}=340/505°C (T_{cr}=374°C); high-temperature steam superheat; or indirect **SCP Rankine "steam" cycle**: P_{in}≈24.5 MPa (P_{cr}=22.064 MPa) and T_{in}/T_{out}=340/520°C (T_{cr}=374°C); also, note that power-conversion cycle in a different LFR designs from other countries is based on **SCP carbon-dioxide Brayton gas-turbine cycle**.	~41–43
6	Sodium-cooled Fast Reactor (SFR) NPP (Russian design BN-600 (see Fig. 4): reactor coolant – liquid sodium (primary circuit): P≈0.1 MPa and T_{in}/T_{out}=380/550°C; liquid sodium (secondary circuit): T_{in}/T_{out}=320/520°C; primary power cycle – indirect Rankine steam cycle: P_{in}≈14.2 MPa (T_{sat}≈337°C) and $T_{in\ max}$=505°C (T_{cr}=374°C); steam superheat: P≈2.45 MPa and T_{in}/T_{out}=246/505°C; possible back-up in some other countries – indirect **SCP carbon-dioxide Brayton gas-turbine cycle**).	~40

Therefore, solid knowledge of specifics of thermophysical properties, heat transfer, and hydraulic resistance (pressure drop) of SCP reactor coolants and / or SCP working fluids in power cycles is very important for safe and reliable operation of Generation-IV nuclear-power reactors and NPPs.

4. SPECIFICS OF THERMOPHYSICAL PROPERTIES AT SUPERCRIITCAL PRESSURES

Prior to a general discussion on specifics of thermophysical properties at subcritical, critical, and supercritical pressures, it is important to define special terms and expressions used at these conditions. For better understanding of these terms and expressions, their definitions are listed below together with complementary Figs. 10–18.

Definitions of General Terms and Expressions Used in this Paper

Compressed fluid is the fluid at a pressure above the critical pressure, but at a temperature below the critical temperature (see Figs. 10 and 11).

Critical point (also called a critical state) is the point in which the distinction between the liquid and gas (or vapor) phases disappears, i.e., both phases have the same temperature, pressure, and specific volume or density (see Figs. 10, 11 and 12b). The critical point is characterized with the phase-state parameters: T_{cr}, P_{cr}, and v_{cr} (or ρ_{cr}), which have unique values for each pure substance.

Near critical point is actually a narrow region around the critical point, where all thermophysical properties of a pure fluid exhibit rapid variations (see Figs. 12b–16).

Overheated vapor is the vapor at pressures below the critical pressure, and at temperatures above the saturation temperature, but below the critical temperature (see Figs. 10 and 11).

Pseudocritical line is the line, which consists of pseudocritical points (see Figs. 10 and 11).

Pseudocritical point (characterized with P and T_{pc}) is the point at a pressure above the critical pressure and at a temperature ($T_{pc} > T_{cr}$) corresponding to the maximum value of specific heat at this particular pressure (see Fig. 14).

Supercritical fluid is the fluid at pressures and temperatures that are higher than the critical pressure and critical temperature (see Figs. 10 and 11). However, in the current paper, the term supercritical fluid usually includes both terms – a supercritical fluid and compressed fluid.

Supercritical "steam" is actually supercritical water, because at supercritical pressures, fluid is considered as a single-phase substance. However, this term is widely (and incorrectly) used in the literature in relation to supercritical-"steam" generators and turbines.

Supercritical vapor is actually supercritical fluid, because at supercritical pressures, fluid is considered as a single-phase substance.

Superheated steam is the steam at pressures below the critical pressure but at temperatures above the critical temperature (see Fig. 10).

Superheated vapor is the vapor at pressures below the critical pressure but at temperatures above the critical temperature (see Fig. 11).

In general, all publications used in the current paper are listed at the end of the paper in the following order: 1) Books [1, 2]; 2) Chapters in books [3–8]; 3) Journal papers [9–17]; 4) Conference papers [18, 19]; 5) Reports [20]; and 6) Additional references [21–24]. All thermophysical properties in the current paper were calculated according to the NIST REFPROP software (2013) [21]. Also, NIST REFPROP can be used for calculation thermophysical properties of 121 pure fluids, including water, carbon dioxide, helium, refrigerants, etc.; 5 pseudo-pure fluids (such as air); and mixtures with up to 20 components at different pressures and temperatures, including critical and supercritical regions. In the current paper only selected properties are shown for SCW and SCP carbon dioxide. For properties of other SCFs, see the following publications:

- Subcritical and SC water, SC carbon dioxide, and SC helium can be found in Handbook of Generation IV Nuclear Reactors (2016) [1].

- Subcritical and SCW, SC carbon dioxide, and SC R-134a can be found in [3].
- Subcritical and SCW, SC carbon dioxide, and SC R-134a can be found in [11].
- SCW and SC R-12 can be found in [7].
- SCW and SC carbon dioxide can be found in [15]. And
- SCW, SC carbon dioxide, SC helium, and SC R-134a can be found in [2].

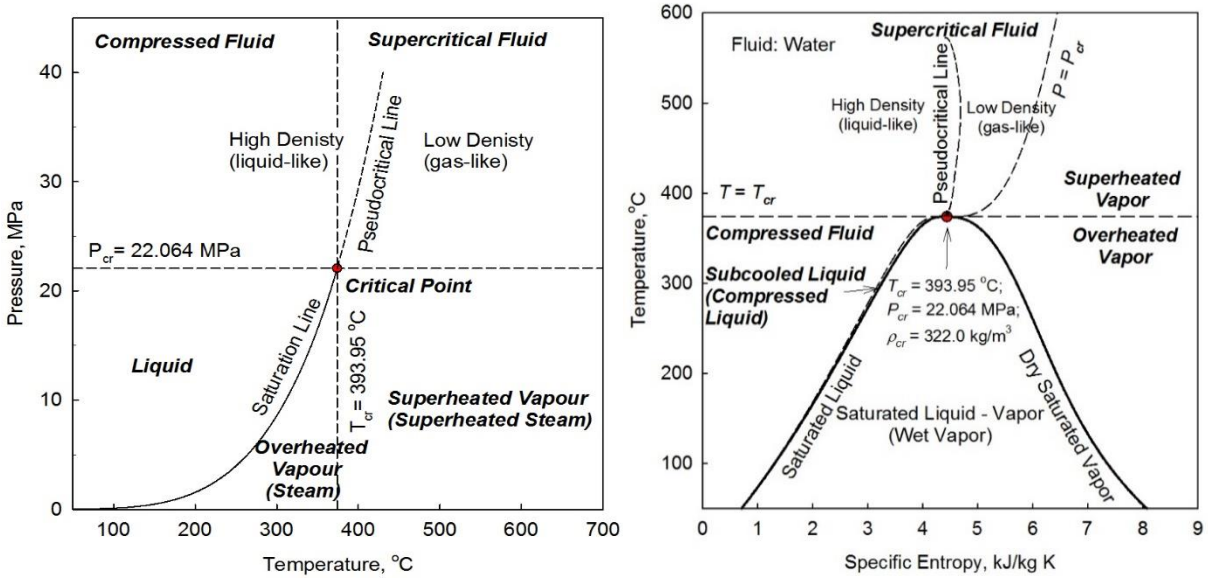

(a) **(b)**

Fig. 10. Thermodynamic diagrams for light water [1]: (a) Pressure–Temperature diagram; and (b) Temperature–Specific-Entropy diagram.

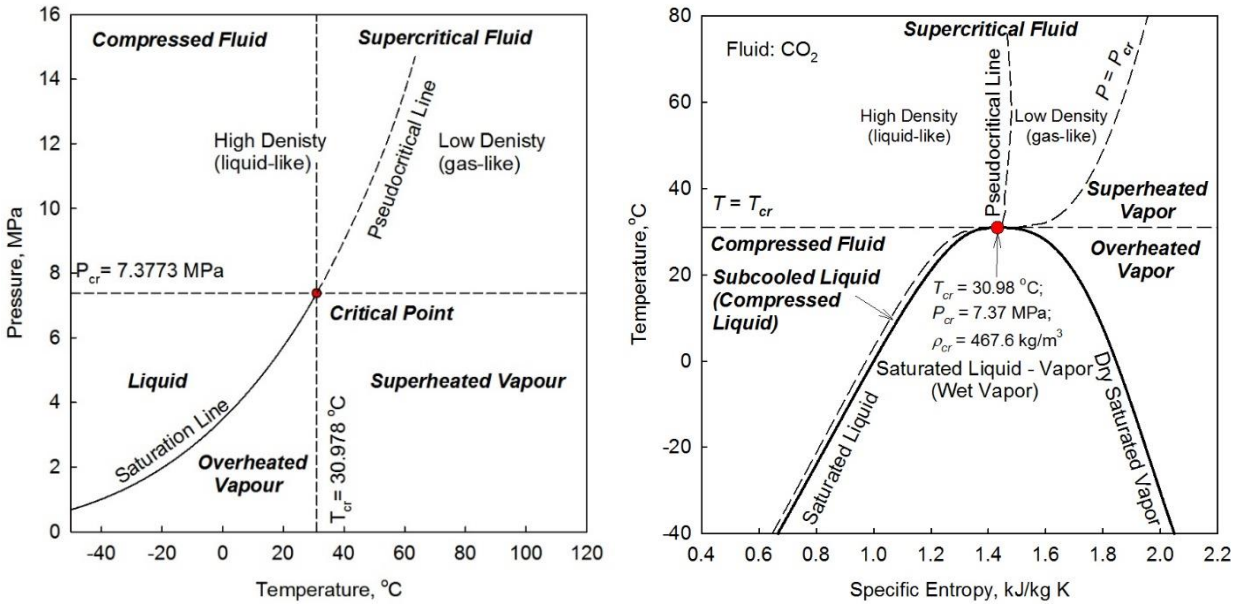

(a) **(b)**

Fig. 11. Thermodynamic diagrams for carbon dioxide [1]: (a) Pressure–Temperature diagram; and (b) Temperature–Specific-Entropy diagram.

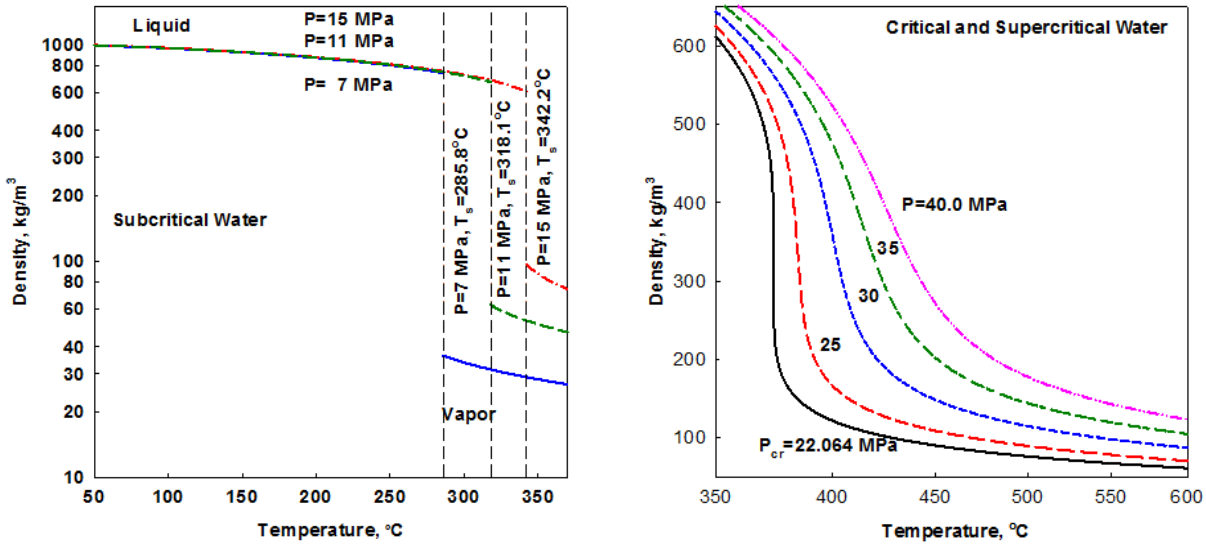

(a) **(b)**

Fig. 12. Density vs. Temperature: (a) Subcritical-pressure water and (b) Critical- and supercritical-pressure water.

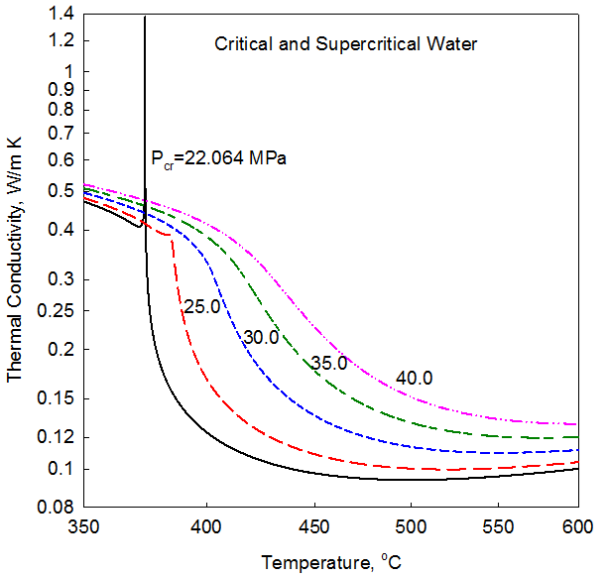

Fig. 13. Thermal Conductivity vs. Temperature of critical and SCW.

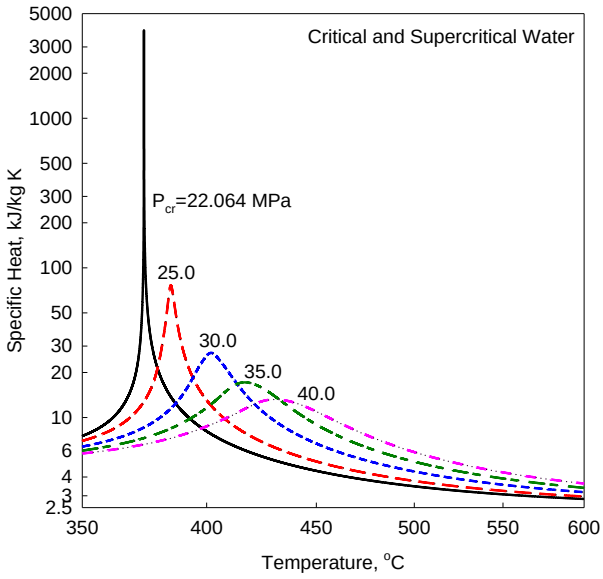

Fig. 14. Specific Heat vs. Temperature of critical and SCW.

Analysis of profiles shown in Fig. 12 for subcritical water (a) and critical/SCW (b) shows similar trends. However, for subcritical water, there are two different values of any thermophysical property on the saturation line: one for liquid and one for vapor (steam). At critical and supercritical pressures, a fluid is considered to be a single-phase substance, i.e., at any critical / SCP, all properties have just a single value for any pressure-temperature combination, in spite of the fact that all thermophysical properties undergo significant changes within the critical and

pseudocritical regions (see Figs. 12b–18). Near the critical point, these changes are dramatic. Within the vicinity of pseudocritical points, with an increase in pressure, these changes become less pronounced.

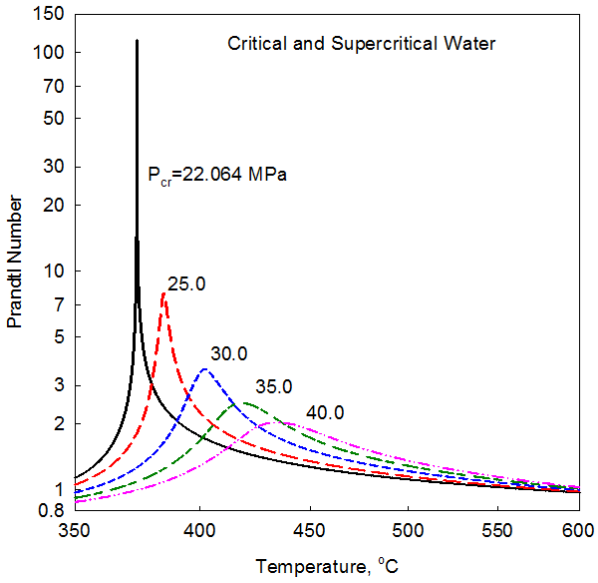

Fig. 15. Prandtl Number vs. Temperature of critical and SCW.

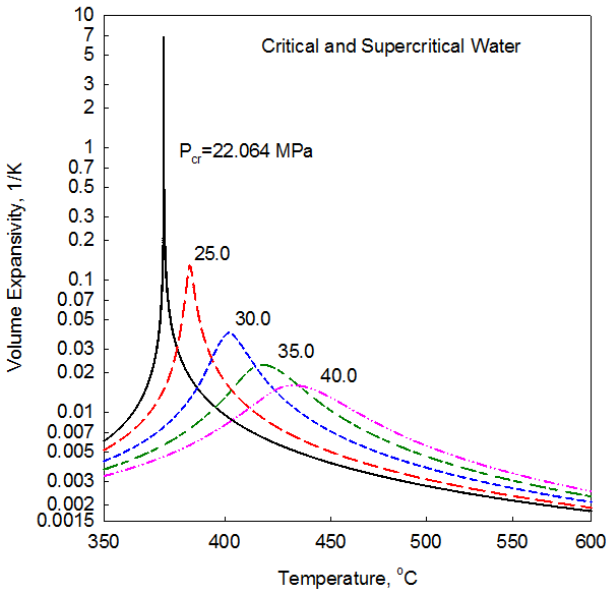

Fig. 16. Volumetric Expansivity vs. Temperature of critical and SCW.

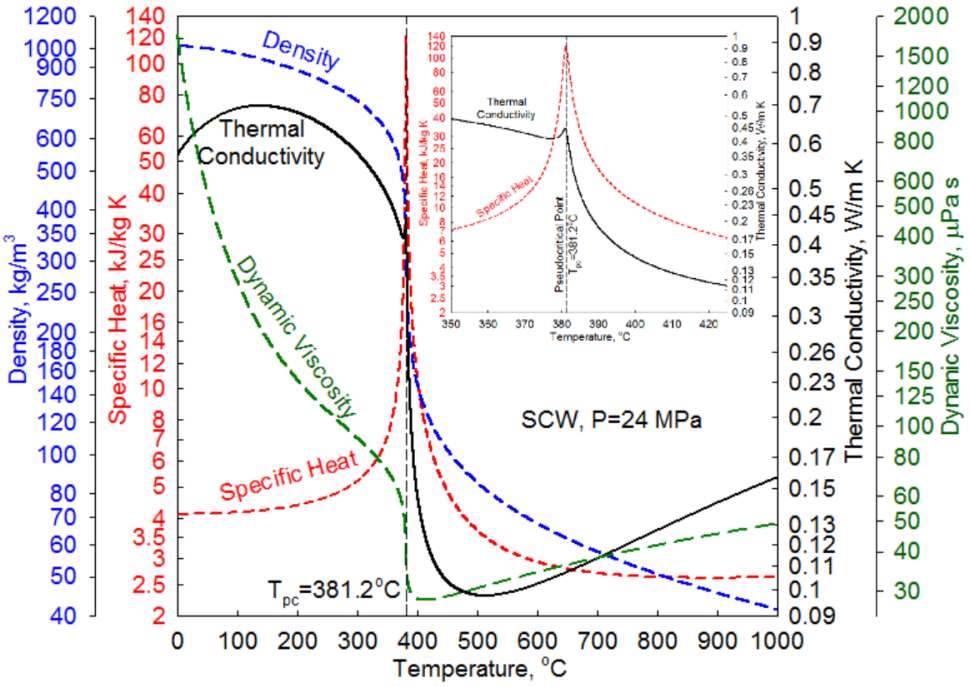

Fig. 17. Density, Specific Heat, Thermal Conductivity, and Dynamic Viscosity vs. Temperature of SCW at 24 MPa. Pseudocritical region is about ±25°C around pseudocritical point.

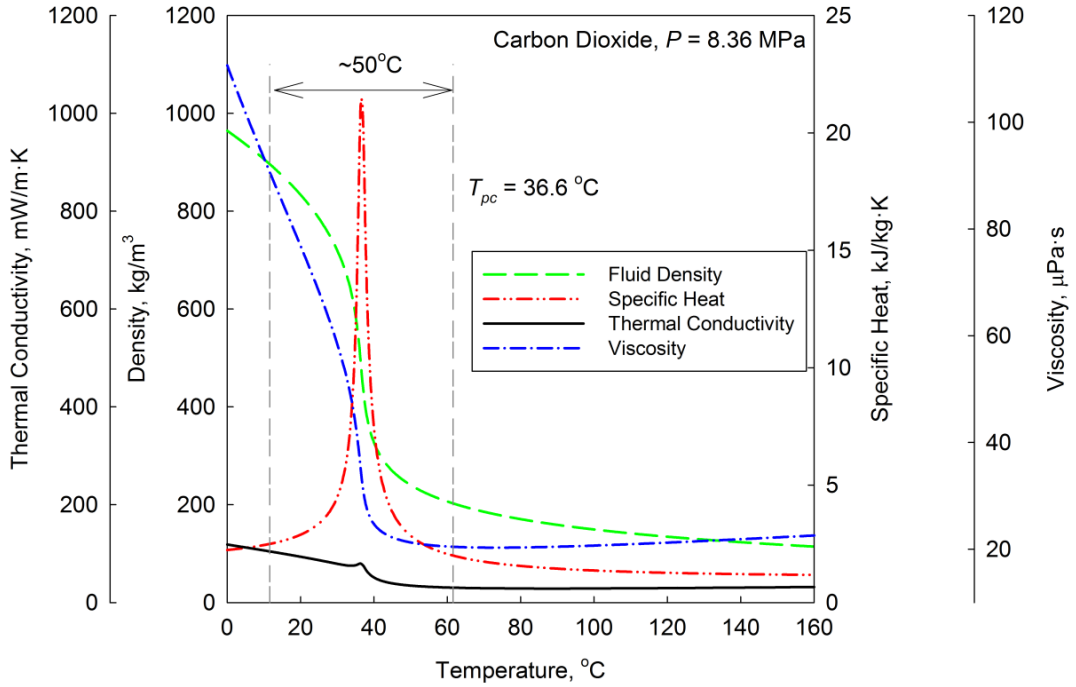

Fig. 18. Thermal Conductivity, Density, Specific Heat, and Dynamic Viscosity vs. Temperature of carbon dioxide at 8.36 MPa (water-equivalent pressure 25 MPa). Pseudocritical region is about ±25°C around pseudocritical point.

It should be noted that for water at pressures approximately above 300 MPa and for carbon dioxide at pressures above 30 MPa, a peak (here, it is better to say a "hump") in the specific heat almost disappears; therefore, the term such as a pseudocritical point no longer exists. The same applies to the pseudocritical line. More details on thermophysical properties at critical and SCPs can be found in [1–4, 6, 7, 11, 15].

5. SPECIFICS OF HEAT TRANSFER AT SUPERCRITICAL PRESSURES

Prior to a general discussion on specifics of heat transfer at critical and supercritical pressures, it is important to define special terms and expressions used at these conditions [1, 2]. For a better understanding of these terms and expressions their definitions are listed below together with Figs. 19–27.

Definitions of Terms and Expressions Related to Critical and Supercritical Regions

Deteriorated Heat Transfer (DHT) is characterized with lower values of the Heat Transfer Coefficient (HTC) compared to those at normal heat transfer; and, hence, has higher values of wall temperature within some part of a test section or within the entire test section (see Figs. 19, and 25–27).

Improved Heat Transfer (IHT) is characterized with higher values of the HTC compared to those at normal heat transfer; and, hence, lower values of wall temperature within some part of a test section or within the entire test section (see Figs. 19, 21, and 26). In our opinion, the improved

heat-transfer regime or mode includes peaks or "humps" in the HTC near the critical or pseudocritical points.

Normal Heat Transfer (NHT) can be characterized in general with HTCs similar to those of subcritical convective heat transfer far from the critical or pseudocritical regions (see Figs. 19–21, 25, and 26), , when they are calculated according to the conventional single-phase Dittus-Boelter-type correlations:

$$\mathbf{Nu} = 0.023\ \mathbf{Re}^{0.8}\mathbf{Pr}^{0.4}. \qquad (1)$$

Pseudo-boiling is a physical phenomenon similar to subcritical-pressure nucleate boiling, which may appear at SCPs. Due to heating of an SCF with a bulk-fluid temperature below the pseudocritical temperature (high-density fluid, i.e., "liquid-like" (see Figs. 10 and 11)), some layers near the heating surface may attain temperatures above the pseudocritical temperature (low-density fluid, i.e., "gas-like"). This low-density "gas-like" fluid leaves the heating surface in a form of variable density (bubble) volumes. During the pseudo-boiling, the HTC usually increases (IHT regime) (see Figs. 19, 21, and 26).

Pseudo-film boiling is a physical phenomenon similar to subcritical-pressure film boiling, which may appear at SCPs. At pseudo-film boiling, a low-density fluid (a fluid at temperatures above the pseudocritical temperature, i.e., "gas-like" (see Figs. 10 and 11)) prevents a high-density fluid (a fluid at temperatures below the pseudocritical temperature, i.e., "liquid-like") from contacting ("rewetting") a heated surface. Pseudo-film boiling leads to the DHT regime (see Figs. 19, and 25–27).

Major problem for using subcritical-pressure forced-convection heat-transfer correlations (see Figs. 19 and 20) is a "peak" (at higher SCPs – a "hump") in the Prandtl-number profile (see Fig. 15), which is due to the corresponding "peak" or "hump" in the specific-heat profile within the pseudocritical region (see Figs. 14, 17, and 18). Experimental data obtained at SCPs show that the HTC profile within the pseudocritical region is affected with heat flux, i.e., at low heat flux HTC profile will also have a "peak" or "hump" (see Figs. 19, 21, and 26), but at high heat flux a "peak" or "hump" will be moved upstream of the pseudocritical point and will be "depressed".

Therefore, to account for significant variations of thermophysical properties within the pseudocritical region and effect of heat flux (which is absent in the Dittus-Boelter (DB) or DB-type correlations (see Eq. (1)) it was proposed: 1) instead of the regular specific heat, c_p, (for example, from the NIST REFPROP [21]), which depends only on temperature and pressure, to use an average in cross-section calculated specific heat, $\bar{c}_p = \left(\dfrac{H_w - H_b}{T_w - T_b} \right)$, and corresponding to that to use an averaged Prandtl number within the range of ($t_w - t_b$), $\overline{\mathbf{Pr}} = \left(\dfrac{\mu\ \bar{c}_p}{k} \right)$; and 2) to use in addition to **Re** and $\overline{\mathbf{Pr}}$ numbers some of the following non-dimensional ratios of thermophysical properties obtained at wall and bulk-fluid temperatures: $\left(\dfrac{\rho_w}{\rho_b}\right)$; $\left(\dfrac{\mu_w}{\mu_b}\right)$; $\left(\dfrac{k_w}{k_b}\right)$; etc. [1, 2, 3, 6, 8, 11, 15, 16, 18, and 20].

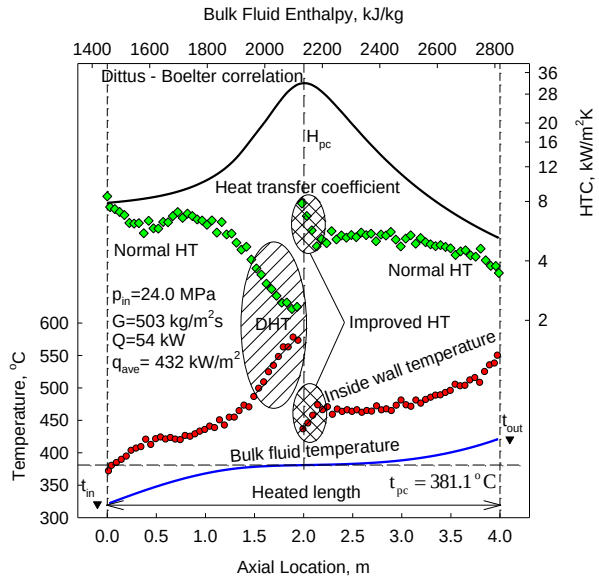

Fig. 19. Temperature and HTC profiles along heated length of vertical bare circular tube (D = 10 mm and L_h = 4 m): SCW; upward flow; P_{in}=~24 MPa; and G = 1500 kg/m^{2}s (experimental data by Kirillov et al. [22]).

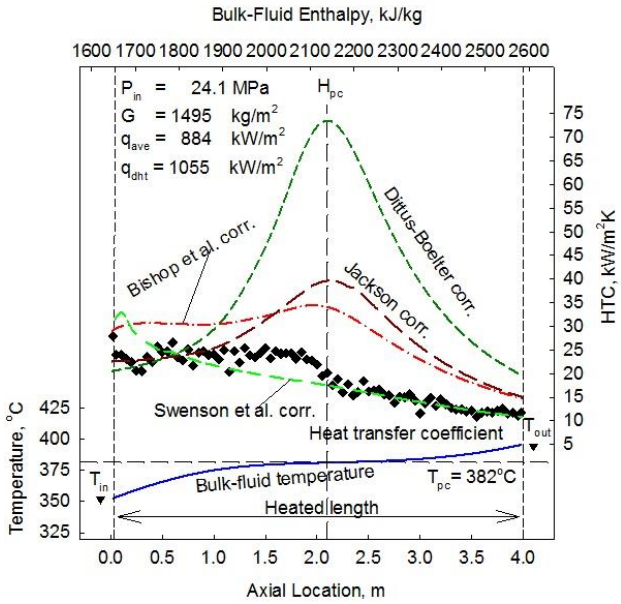

Fig. 20. Comparison of HTC values calculated through various correlations with experimental data obtained in vertical bare circular tube (D = 10 mm and L_h = 4 m) [16]: SCW, upward flow; P_{in}=~24 MPa and G = 1500 kg/m^{2}s (experimental data by Kirillov et al. [22]).

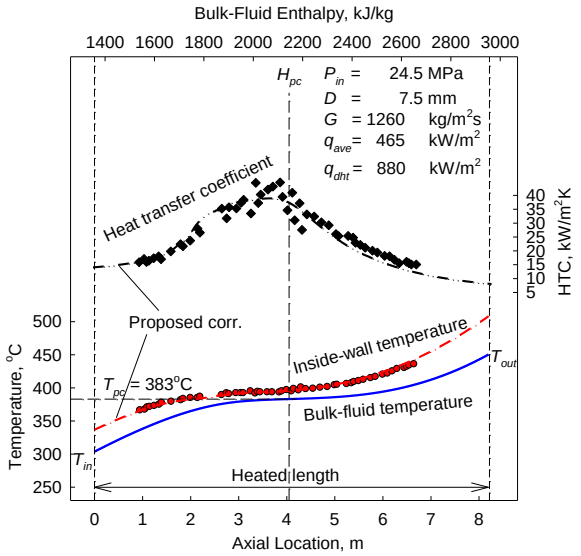

Fig. 21. Temperature and HTC profiles along vertical bare circular tube at various heat fluxes: SCW, P_{in}=24.5 MPa and D=7.5 mm (experimental data from [21]; proposed correlation – Mokry et al. [16]).

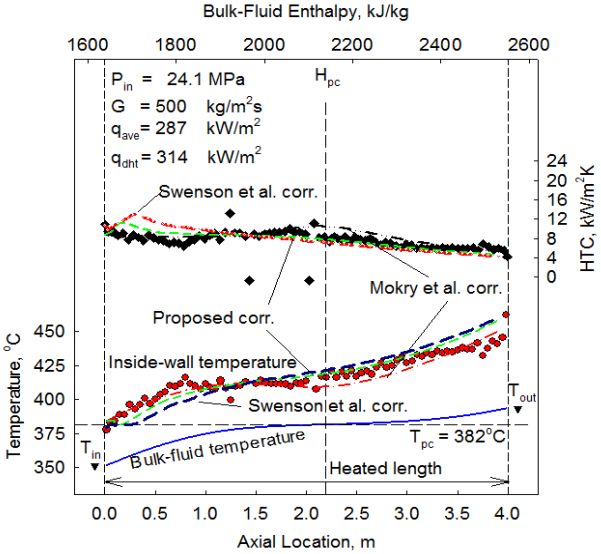

Fig. 22. Temperature and HTC profiles at various heat fluxes along vertical bare circular tube (D = 10 mm and L_h=4 m) [13]: SCW, P_{in} = 24.0 MPa and G = 500 kg/m^{2}s (experimental data by Kirillov et al. [22]; proposed correlation – Gupta et al. [13]).

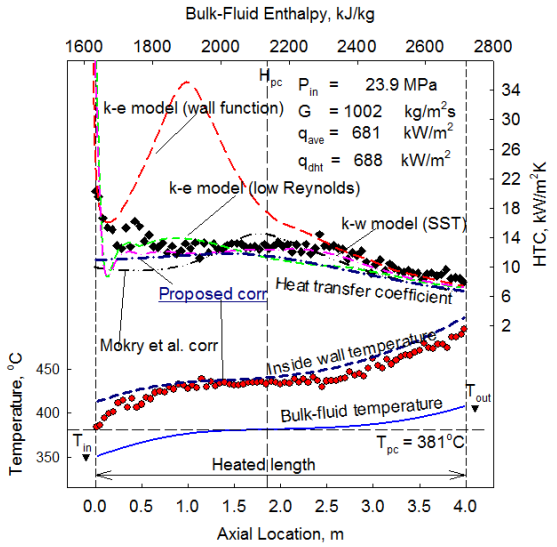

Fig. 23. Comparison of HTC and wall-temperature values calculated with proposed correlation (Gupta et al. [13]) and FLUENT CFD code with experimental data obtained in vertical bare circular tube (*D* = 10 mm and L_h=4 m) [13]: SCW, P_{in} = 24 MPa and *G* = 1000 kg/m²s (experimental data by Kirillov et al. [22]).

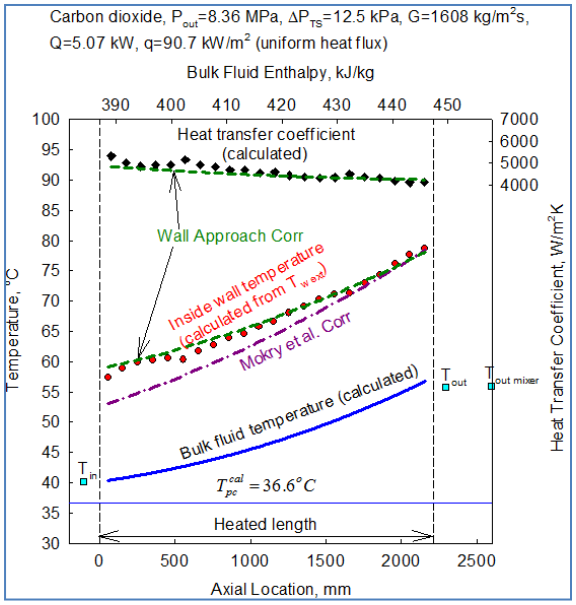

Fig. 24. Temperature and HTC profiles along vertical bare circular tube (*D*=8 mm and L_h=2.208 m) [19]: SC CO_2, *P*=8.4 MPa; *G*=1608 kg/m²s; and *q*=90.7 kW/m²; (experimental data by Pioro et al. [19]; proposed correlation – Gupta et al. [13]).

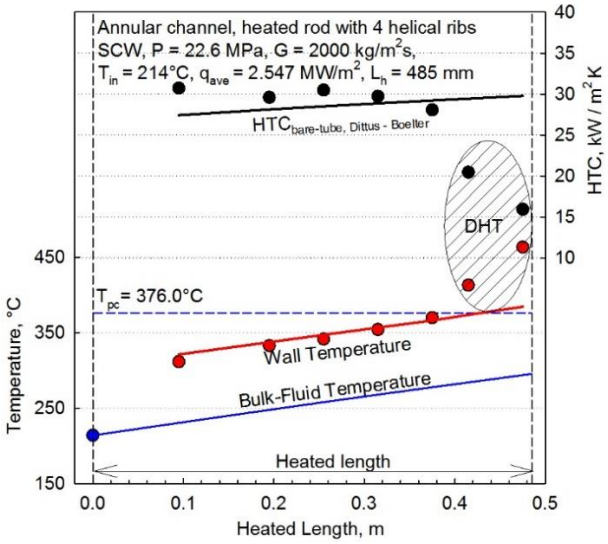

Fig. 25. Temperature and HTC profiles along heated length of vertical annular channel with rod equipped with four helical ribs: SCW and upward flow.

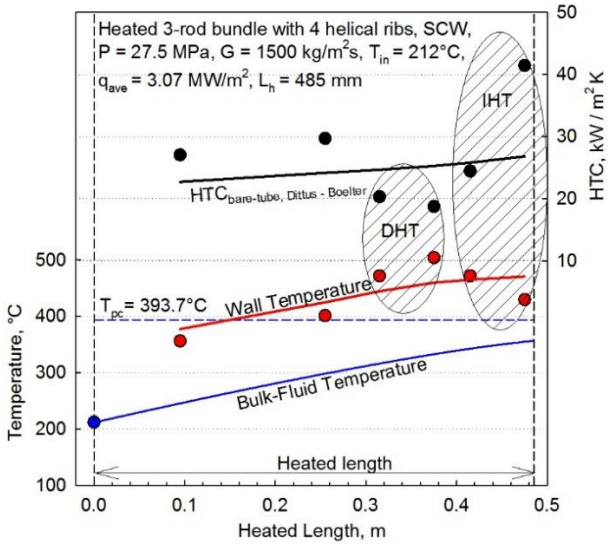

Fig. 26. Temperature and HTC profiles along heated length of vertical 3-rod bundle (rods equipped with four helical ribs): SCW and upward flow.

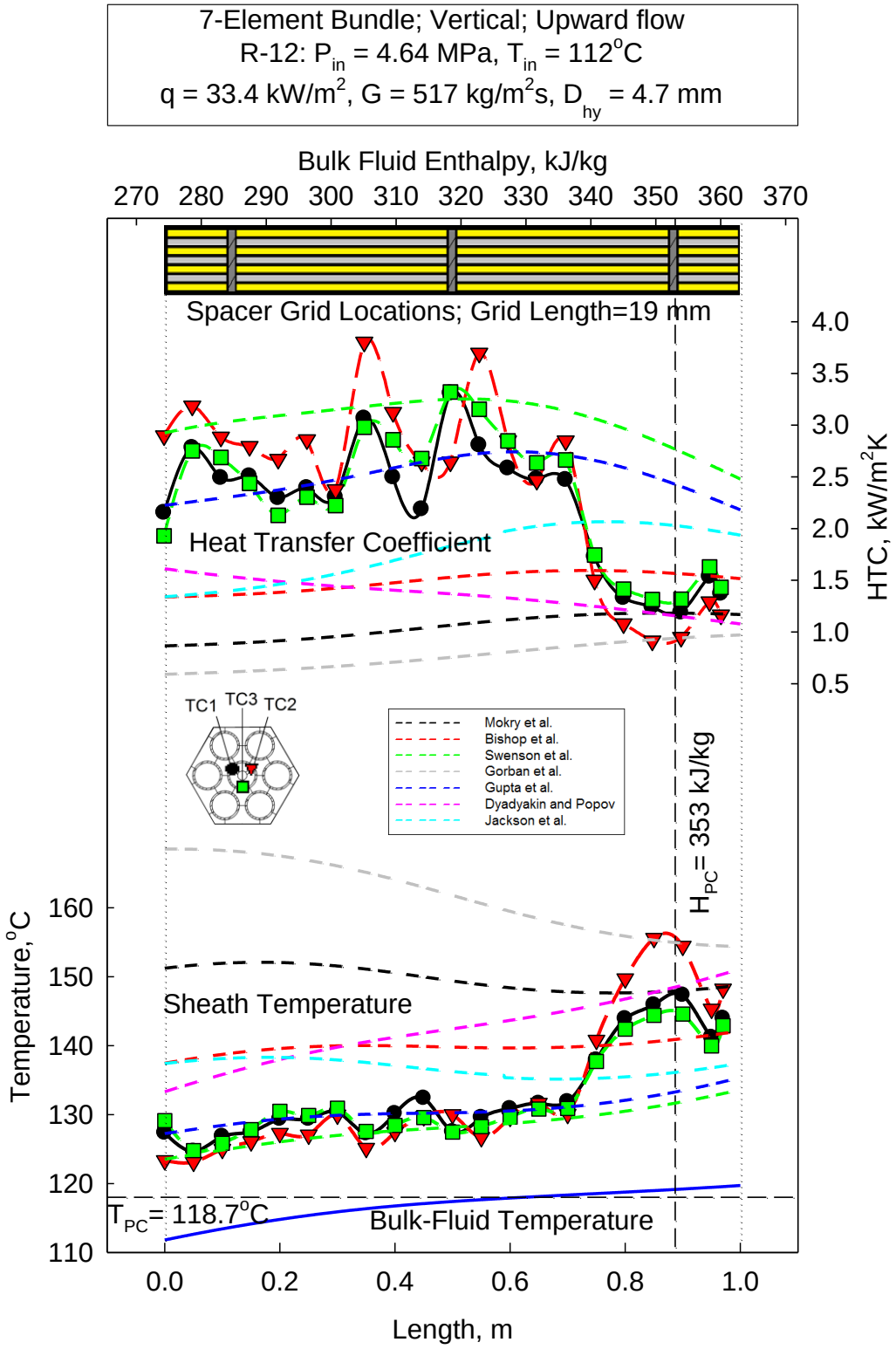

Fig. 27. Comparison of HTC and wall-temperature values calculated with various correlations with experimental data obtained in vertical bare 7-element bundle [14]: SC R-12; upward flow; P_{in} = 24 MPa and G = 1000 kg/m²s (experimental data by Kirillov et al.). DHT regime is visible within heated length of 0.75–1.0 m.

It should be noted that SCP heat-transfer correlations, which contain thermophysical properties at two different temperatures, require iterations to be solved, because there are two unknowns: 1) HTC and 2) wall or film[4] temperature. Therefore, the initial wall-temperature value at which fluid properties will be estimated should be "guessed" to start iterations.

The majority of SCP heat-transfer empirical correlations were proposed in the 1960s – 1970s [2, 18, 20], when experimental techniques were not at the same level (i.e., advanced level) as of today. Also, thermophysical properties of water and other SCFs have been updated since that time (for example, a peak in thermal conductivity in critical and pseudocritical points within a range of pressures from 22.1 to 25 MPa for water was not officially recognized until the 1990s).

Therefore, recently new correlations, based on a new set of heat-transfer data and the latest thermophysical properties of SCW [16, 11], SC carbon dioxide, and other SCFs were developed and evaluated. The following correlations – Eqs. (2) – (6) have been developed by Dr. I. Pioro with his students.

Correlation for SCW, which is based on the bulk-fluid-temperature approach and cross-section-averaged specific heat / **Pr** number (Mokry et al. (2011) [16]), is as the following:

$$\mathbf{Nu_b} = 0.0061\ \mathbf{Re_b^{0.904}}\ \overline{\mathbf{Pr}}_\mathbf{b}^{0.684}\left(\frac{\rho_w}{\rho_b}\right)^{0.564} \quad (2)$$

Correlation (Eq. (2)) is the most accurate heat-transfer correlation for SCW forced convection compared to other 14 heat-transfer correlations: Uncertainty ±25% for HTC values and ±15% for wall temperatures (this statement is based on references [18, 20]). This correlation was verified within the following operating conditions: SCW, upward flow, vertical bare tubes with inside diameters of 3 – 38 mm, pressures 22.8 – 29.4 MPa, mass fluxes 200 – 3000 kg/m^{2}s, and heat fluxes 70 – 1250 kW/m^2. Also, Eq. (2) showed very good predictions for subcritical liquids and the most accurate for superheated steam compared to other four correlations [18].

Correlation for SCW, which is based on the wall-temperature approach and cross-section-averaged specific heat / **Pr** number (Gupta et al., (2011) [18]), is as the following:

$$\mathbf{Nu_w} = 0.0033\ \mathbf{Re_w^{0.941}}\ \overline{\mathbf{Pr}}_\mathbf{w}^{0.764}\left(\frac{\mu_w}{\mu_b}\right)^{0.398}\left(\frac{\rho_w}{\rho_b}\right)^{0.156} \quad (3)$$

Correlation (Eq. (3)) is also the most accurate heat-transfer correlation for SCW forced convection compared to other 14 heat-transfer correlations (the uncertainty is the same as that for Eq. (2)) [18, 20]. And this correlation was verified within the same operating conditions as those for Eq. (2), and is .applicable for NHT and IHT regimes.

However, it should be noted that both correlations, i.e., Eqs. (2) and (3), as well as many other SCFs heat-transfer correlations, can predict only HTC values at NHT and IHT regimes. Unfortunately, there are no reliable correlations to predict HTCs at the DHT regime.

[4] Film temperature is the arithmetic average temperature between bulk-fluid and wall temperatures.

Nevertheless, the following empirical correlation for SCW was proposed for calculating the minimum heat flux at which the DHT regime appears in forced convection in bare vertical tubes with upward flow (Mokry et al., (2011) [16]:

$$q_{dht} = -58.97 + 0.745 \cdot G, \text{ kW/m}^2. \quad (4)$$

Correlation (Eq. (4)) is valid within the following range of experimental parameters: SCW, upward flow, vertical bare tube with inside diameter of 10 mm, pressure 24 MPa, mass flux 200 – 1500 kg/m^{2}s, and bulk-fluid inlet temperature 320 – 350°C: Uncertainty ±15% for the DHT heat flux.

Correlation for SC carbon dioxide, which is based on wall-temperature approach and cross-section-averaged specific heat (Gupta et al., (2013) [11]):

$$\mathbf{Nu_w} = 0.0038\, \mathbf{Re_w^{0.957}}\, \overline{\mathbf{Pr_w}}^{-0.14} \left(\frac{\rho_w}{\rho_b}\right)^{0.84} \left(\frac{k_w}{k_b}\right)^{-0.75} \left(\frac{\mu_w}{\mu_b}\right)^{-0.22} \quad (5)$$

Correlation (Eq. (5)) is the heat-transfer correlation for SC carbon-dioxide forced convection: Uncertainty ±30% for HTC values and ±20% for wall temperatures (see Fig. 24). This correlation was verified within the following operating conditions: Carbon dioxide, upward flow, vertical bare tube with inside diameter 8 mm; pressure 7.6 – 8.8 MPa, mass flux 700 – 3170 kg/m^{2}s, heat flux 10 – 615 kW/m^2, inlet temperature 20 – 40°C, and outlet temperature 30 – 225°C.

The following empirical correlation for SC carbon dioxide was proposed for calculating the minimum heat flux at which the DHT regime appears in forced convection in bare vertical tubes with upward flow (Saltanov et al., 2015):

$$q_{dht} = 66.81 + 0.18 \cdot G, \text{ kW/m}^2. \quad (6)$$

Correlation (Eq. (6)) is valid within the following range of experimental parameters: SC carbon dioxide, upward flow, vertical bare tube with inside diameter 8 mm, pressure 7.6 – 8.8 MPa, mass flux 890 – 2990 kg/m^{2}s, and bulk-fluid inlet temperature 20 – 35°C. The RMS error is about 9%.

Correlations (Eqs. (1) – (3) and (5)) can be applied not only for circular tubes, but for any other flow geometries through using the hydraulic-equivalent diameter $\left(D_{hy} = \frac{4 \cdot A_{fl}}{p_{wet}}\right)$ instead of an inside-tube diameter in Nusselt and Reynolds numbers. Moreover, Eqs. (2) and (3) can be used for bundle flow geometries as a conservative approach, because in bundles HTCs are usually higher than those in bare tubes due to various appendages, grids, endplates, spacers, etc., which turbulize flow and enhance heat transfer.

It should be noted that empirical correlations (Eqs. (2), (3) and (5)) can be used only within the tested ranges, because at heat fluxes beyond the tested ones these correlations might not be converged.

Figures 25–27 show experimental data obtained in annulus cooled with SCW (Fig. 25), and bundles cooled with SCW (Fig. 26) and SC R-12 (Fig. 27). Data in Figs. 25 – 26 show that all three HT regimes can be found in other flow geometries. Also, data in Figs. 25 and 26 show that

the Dittus-Boelter correlations can be used to predict these HT data quite closely below the pseudocritical point.

Analysis of the data in Table 5 shows that q_{DHT} values in bare tubes are significantly lower (up to 1.8 times) than those in the single-rod annulus and 3-rod bundle.

Table 5. Comparison between onset of DHT between bare-tube, annular channel, and 3-rod bundle.

No	Test section	Operating Conditions	q_{DHT}, MW/m^2
1	Bare-tube	P = 24.1 MPa and G = 2000 kg/m^{2}s	1.43
2	Single-rod annulus	P = 22.6 MPa and G = 2000 kg/m^{2}s	2.55
3	Bare-tube	P = 24.1 MPa and G = 2700 kg/m^{2}s	1.95
4	3-rod bundle	P = 22.6 MPa and G = 2700 kg/m^{2}s	3.20

6. HYDRAULIC RESISTANCE

In general, the total pressure drop for forced convection flow inside a test section, installed in a closed-loop system, can be calculated according to the following expression [1, 2, 17]:

$$\Delta p = \sum \Delta p_{fr} + \sum \Delta p_{\ell} + \sum \Delta p_{ac} + \sum \Delta p_{g} , \tag{7}$$

where Δp is the total pressure drop, Pa.

Δp_{fr} is the pressure drop due to frictional resistance (Pa), which defined as:

$$\Delta p_{fr} = \left(\xi_{fr} \frac{L}{D} \frac{\rho u^2}{2} \right) = \left(\xi_{fr} \frac{L}{D} \frac{G^2}{2\rho} \right), \tag{8}$$

where ξ_{fr} is the frictional coefficient, which can be obtained from appropriate correlations for different flow geometries. For smooth circular tubes ξ_{fr} is as follows (Filonenko, 1954):

$$\xi_{fr} = \left(\frac{1}{\left(1.82 \log_{10} \mathbf{Re_b} - 1.64\right)^2} \right). \tag{9}$$

Equation (9) is valid within a range of $\mathbf{Re} = 4 \cdot 10^3 - 10^{12}$.

Usually, thermophysical properties and the Reynolds number in Eqs. (8) and (9) are based on arithmetic average of inlet and outlet values.

Δp_{ℓ} is the pressure drop due to local flow obstruction (Pa), which is defined as

$$\Delta p_{\ell} = \left(\xi_{\ell} \frac{\rho u^2}{2} \right) = \left(\xi_{\ell} \frac{G^2}{2\rho} \right), \tag{10}$$

where ξ_{ℓ} is the local resistance coefficient, which can be obtained from appropriate correlations for different flow obstructions.

Δp_{ac} is the pressure drop due to acceleration of flow (Pa) defined as

$$\Delta p_{ac} = \left(\rho_{out} u_{out}^2 - \rho_{in} u_{in}^2 \right) = G^2 \left(\frac{1}{\rho_{out}} - \frac{1}{\rho_{in}} \right). \tag{11}$$

Δp_g is the pressure drop due to gravity (Pa) defined as

$$\Delta p_g = \pm g \left(\frac{\rho_{out} + \rho_{in}}{2} \right) L \sin\theta , \tag{12}$$

where θ is the test-section inclination angle to the horizontal plane, sign "+" is for the upward flow and sign "–" is for the downward flow. The arithmetic average value of densities can be used only for short sections in the case of strongly non-linear dependency of the density versus temperature. Therefore, in long test sections at high heat fluxes and within the critical and pseudocritical regions, the integral value of densities should be used (see Eq. (16)).

Ornatskiy et al. (1980) and Razumovskiy (2003) proposed to calculate Δp_g at supercritical pressures as the following:

$$\Delta p_g = \pm g \left(\frac{H_{out}\ \rho_{out} + H_{in}\ \rho_{in}}{H_{out} + H_{in}} \right) L \sin\theta . \tag{13}$$

NOMENCLATURE

A flow area, m^2

c_p specific heat at constant pressure, J/kg K

$\bar{c}_p$ averaged specific heat within range of $(t_w - t_b)$; $\left(\frac{H_w - H_b}{T_w - T_b} \right)$, J/kg K

D inside diameter, m

D_{hy} hydraulic-equivalent diameter $\left(\frac{4 \cdot A_{fl}}{p_{wet}} \right)$

G mass flux, kg/m^{2}s; $\left(\frac{m}{A_{fl}} \right)$

g gravitational acceleration, m/s^2

H specific enthalpy, J/kg

h heat transfer coefficient, W/m^{2}K

k thermal conductivity, W/m K

L heated length, m

m mass-flow rate, kg/s; (ρV)

P, p pressure, MPa

p_{wet} wetted perimeter, m

Q heat-transfer rate, W

q heat flux, W/m^2; $\left(\frac{Q}{A_h} \right)$

s specific entropy, J/kg K

T, t temperature, ºC

u axial velocity, m/s

V volume-flow rate, m^3/kg

v specific volume, m^3/kg; $1/\rho$

Greek Letters

α thermal diffusivity, m^2/s; $\left(\frac{k}{c_p\ \rho} \right)$

Δ difference

θ test-section inclination angle

μ dynamic viscosity, Pa s

ξ friction coefficient

ρ density, kg/m^3

υ kinematic viscosity, m^2/s

Non-dimensional Numbers

Nu Nusselt number; $\left(\frac{h\ D}{k} \right)$

Pr Prandtl number; $\left(\frac{\mu\ c_p}{k} \right) = \left(\frac{\upsilon}{\alpha} \right)$

$\overline{\mathbf{Pr}}$ averaged Prandtl number within range of $(t_w - t_b)$; $\left(\frac{\mu\ \bar{c}_p}{k} \right)$

Re Reynolds number; $\left(\frac{G\ D}{\mu} \right)$

Subscripts or superscripts

ac acceleration

ave average

b bulk

cr critical

dht deteriorated heat transfer

fl flow

fr friction

g gravitational

h heated

hy	hydraulic-equivalent
in	inlet
ℓ	local
out	outlet or outside
pc	pseudocritical
sat	saturation
w	wall

Abbreviations and acronyms

AGR	Advanced Gas-cooled Reactor
BN	Fast Sodium (in Russian abbreviations)
DHT	Deteriorated Heat Transfer
EEC	Electrical Energy Consumption
GFR	Gas-cooled Fast Reactor
GIF	Generation-IV International Forum
HDI	Human Development Index
HT	Heat Transfer
HTC	Heat Transfer Coefficient
IAEA	International Atomic Energy Agency
ID	Inside Diameter
IHT	Improved Heat Transfer
LFR	Lead-cooled Fast Reactor
MSR	Molten Salt Reactor
NHT	Normal Heat Transfer
NIST	National Institute of Standards and Technology (USA)
NPP	Nuclear Power Plant
PWR	Pressurized Water Reactor
RMS	Root Mean Square (error)
SC	SuperCritical
SCF	SuperCritical Fluid
SCP	SuperCritical Pressure
SCW	SuperCritical Water
SCWR	SuperCritical Water-cooled Reactor
SFR	Sodium-cooled Fast Reactor
VHTR	Very High Temperature Reactor

REFERENCES

Books

[1] Handbook of Generation IV Nuclear Reactors, 2016. Editor: I.L. Pioro, Elsevier – Woodhead Publishing (WP), Duxford, UK, 940 pages. Free download of content: https://www.gen-4.org/gif/jcms/c_9373/publications.

[2] Pioro, I.L. and Duffey, R.B., 2007. Heat Transfer and Hydraulic Resistance at Supercritical Pressures in Power Engineering Applications, ASME Press, New York, NY, USA, 334 pages.

Chapters in books

[3] Pioro, I., Mahdi, M., and Popov, R., 2017. Heat-Transfer Media and Their Properties, (100 pages), Chapter in: Handbook of Thermal Science and Engineering, Editors: F.A. Kulacki, R. Cotta, and K. Vafai, Springer.

[4] Pioro, I., Mahdi, M., and Popov, R., 2017. Application of Supercritical Fluids in Power Engineering, (pp. 404-457), Chapter 13 in book: Advanced Applications of Supercritical Fluids in Energy Systems, Editors: L. Chen and Yu. Iwamoto, IGI Global, Hershey, PA, USA, 626 pages.

[5] Pioro, I. and Kirillov, P., 2013. Generation IV Nuclear Reactors as a Basis for Future Electricity Production in the World, Chapter in the book: Materials and Processes for Energy: Communicating Current Research and Technological Developments, Energy Book Series #1, Editor: A. Méndez-Vilas, Publisher: Formatex Research Center, Spain, pp. 818-830. Free download from: http://www.formatex.info/energymaterialsbook/book/818-830.pdf.

[6] Pioro, I., 2011. The Potential Use of Supercritical Water-Cooling in Nuclear Reactors. Chapter in Nuclear Energy Encyclopedia: Science, Technology, and Applications, Editors: S.B. Krivit, J.H. Lehr and Th.B. Kingery, J. Wiley & Sons, Hoboken, NJ, USA, pp. 309-347.

[7] Pioro, I. and Mokry, S., 2011. Thermophysical Properties at Critical and Supercritical

Conditions, Chapter in book "Heat Transfer. Theoretical Analysis, Experimental Investigations and Industrial Systems", Editor: A. Belmiloudi, INTECH, Rijeka, Croatia, pp. 573-592. Free download from: http://www.intechopen.com/books/heat-transfer-theoretical-analysis-experimental-investigations-and-industrial-systems/thermophysical-properties-at-critical-and-supercritical-pressures.

[8] Pioro, I. and Mokry, S., 2011. Heat Transfer to Fluids at Supercritical Pressures, Chapter in book "Heat Transfer. Theoretical Analysis, Experimental Investigations and Industrial Systems", Editor: A. Belmiloudi, INTECH, Rijeka, Croatia, pp. 481-504. Free download from: http://www.intechopen.com/books/heat-transfer-theoretical-analysis-experimental-investigations-and-industrial-systems/heat-transfer-to-supercritical-fluids.

Journal papers

[9] Farah, A., Harvel, G., and Pioro, I., 2016. Analysis of CFD Code FLUENT Capabilities for Supercritical Water Heat Transfer Applications in Vertical Bare Tubes, ASME Journal of Nuclear Eng. and Radiation Science, Vol. 2, No. 3, 12 pages.

[10] Razumovskiy, V.G., Pis'mennyi, Eu.N., Sidawi, K., Pioro, I.L., and Koloskov, A.Eu., 2016. Experimental Heat Transfer in an Annular Channel and 3-Rod Bundle Cooled With Upward Flow of Supercritical Water, ASME Journal of Nuclear Eng. and Radiation Science, Vol. 2, No. 1, 8 pages.

[11] Gupta, S., Saltanov, Eu., Mokry, S.J., Pioro, I., Trevani, L. and McGillivray, D., 2013. Developing Empirical Heat-Transfer Correlations for Supercritical CO_2 Flowing in Vertical Bare Tubes, Nuclear Eng. and Design, Vol. 261, pp. 116-131.

[12] Peiman, W., Pioro, I., and Gabriel, K., 2015. Thermal-hydraulic and Neutronic Analysis of a Re-Entrant Fuel Channel Design for Pressure-Channel Supercritical Water-cooled Reactors, ASME Journal of Nuclear Eng. and Radiation Science, Vol. 1, No. 2, 10 pages.

[13] Miletić, M., Růžičková, M., Fukač, R., Pioro, I. and Peiman, W., 2013. Supercritical-Water Experimental Setup for In-Pile Operation, Nuclear Eng. and Design, Vol. 259, pp. 166-171.

[14] Richards, G., Harvel, G.D., Pioro, I.L., Shelegov, A.S. and Kirillov, P.L., 2013. Heat Transfer Profiles of a Vertical, Bare, 7-Element Bundle Cooled with Supercritical Freon R-12, Nuclear Eng. and Design, Vol. 264, pp. 246-256.

[15] Pioro, I., Mokry, S. and Draper, Sh., 2011. Specifics of Thermophysical Properties and Forced-Convective Heat Transfer at Critical and Supercritical Pressures, Reviews in Chemical Eng., Vol. 27, Issue 3-4, pp. 191–214.

[16] Mokry, S., Pioro, I.L., Farah, A., King, K., Gupta, S., Peiman, W. and Kirillov, P., 2011. Development of Supercritical Water Heat-Transfer Correlation for Vertical Bare Tubes, Nuclear Eng. and Design, Vol. 241, pp. 1126-1136.

[17] Pioro, I., Duffey, R. and Dumouchel, T., 2004. Hydraulic Resistance of Fluids Flowing in Channels at Supercritical Pressures (Survey), Nuclear Eng. and Design, Vol. 231, No. 2, pp. 187–197.

Conference papers

[18] Zahlan, H., Groeneveld, D.C., Tavoularis, S., Mokry, S. and Pioro, I., 2011. Assessment of Supercritical Heat Transfer Prediction Methods, Proc. of 5th Int. Symp. on SCWR (ISSCWR-5), Vancouver, BC, Canada, March 13-16, Paper P008, 20 pages.

[19] Pioro, I.L. and Khartabil, H.F., 2005. Experimental Study on Heat Transfer to Supercritical Carbon Dioxide Flowing Upward in a Vertical Tube, Proc. of 13th Int. Conf. on Nuclear Eng. (ICONE-13), Beijing, China, May 16–20, Paper #50118, 9 pages.

Reports

[20] Heat Transfer Behaviour and Thermohydraulics Code Testing for Supercritical Water Cooled Reactors (SCWRs), 2014. IAEA TECDOC Series, IAEA-TECDOC-1746, September, Vienna, Austria, 496 pages. Free download from: http://www-pub.iaea.org/books/IAEABooks/10731/Heat-Transfer-Behaviour-and-Thermohydraulics-Code-Testing-for-Supercritical-Water-Cooled-Reactors-SCWRs.

Additional references

[21] National Institute of Standards and Technology, 2013. NIST Reference Fluid Thermodynamic and Transport Properties-REFPROP. NIST Standard Reference Database 23, Ver. 9.1. Department of Commerce, Boulder, CO, US.

[22] Kirillov, P.L., Opanasenko, A.N., Pometko, R., and Shelegov, A., 2006. Experimental Study of Heat Transfer on Rod Bundle at Supercritical Parameters of Freon-12, (In Russian), IPPE Preprint, Obninsk.

[23] Kirillov, P.L., Lozhkin, V.V., and Smirnov, A.M., 2003. Investigation of Borders of Deteriorated Regimes of a Channel at Supercritical Pressures, (In Russian), State Scientific Center of Russian Federation Institute of Physics and Power Eng. by A.I. Leypunskiy (IPPE), FEI-2988, Obninsk, Russia, 20 pages.

[24] Yamagata, K., Nishikawa, K., Hasegawa, S., et al., 1972. Forced Convective Heat Transfer to Supercritical Water Flowing in Tubes, Int. J. of Heat and Mass Transfer, 15(12), pp. 2575-2593.